

The Reconstruction and Extension of Terrestrial Water Storages Based On A Combined Prediction Model

Erhao Meng

Xi'an University of Technology

Shengzhi Huang (✉ huangshengzhi7788@126.com)

Xi'an University of Technology <https://orcid.org/0000-0001-7592-5268>

Qiang Huang

Xi'an University of Technology

Linyin Cheng

University of Arkansas Fayetteville

Wei Fang

Xi'an University of Technology

Research Article

Keywords: GRACE, Total water storage anomalies, Support vector machine, Combined prediction model, Input selection strategy

Posted Date: July 6th, 2021

DOI: <https://doi.org/10.21203/rs.3.rs-531840/v1>

License:  This work is licensed under a Creative Commons Attribution 4.0 International License.

[Read Full License](#)

1 **The reconstruction and extension of terrestrial**
2 **water storages based on a combined prediction**
3 **model**

4 **Erhao Meng^{a,b}, Shengzhi Huang^{a*1}, Qiang Huang^a, Linyin Cheng^b and Wei**
5 **Fang^a**

6
7
8
9
10 ^a State Key Laboratory Base of Eco-Hydraulic Engineering in Arid Area, Xi'an
11 University of Technology, Xi'an 710048, China

12 ^b Geosciences Department, University of Arkansas, 216C Gearhart Hall, 72701, USA

13
14
15
16
17
18
19
20

*Corresponding author at: State Key Laboratory Base of Eco-Hydraulic Engineering in Arid Area, Xi'an University of Technology, Xi'an 710048, China. Tel.: +86 29 82312801; fax: +86 29 82312797. E-mail Address: huangshengzhi7788@126.com.

21 **Abstract** The monthly changes in total water storage (Δ TWS) can be employed for
22 drought and flood monitoring and early warning and can be obtained from the total
23 water storage anomalies (TWSA) of the Gravity Recovery and Climate Experiment
24 (GRACE). However, the relatively short GRACE time series limits its further wide
25 application. To this end, a combined prediction (CP) model including Support Vector
26 Machine (SVM) and Artificial Neural Network (ANN) was proposed in this study for
27 the reconstruction and extension of monthly TWSA from 1960 to 2012. Moreover, an
28 innovative input selection strategy is proposed to build a monthly TWSA prediction
29 model, in which the partial correlation algorithm is used to select the best input
30 variables from candidate input variables. These candidate input variables include
31 streamflow, precipitation, evaporation, and soil moisture storage (SMS). The Yunnan
32 province, a typical humid area in China, was selected as a case study. The results show
33 that: (1) The innovative input selection strategy effectively improves the simulation
34 ability of the model, especially when the candidate input variables influence each other;
35 (2) The performance of the CP model using the innovative input selection strategy is
36 best; (3) The monthly Δ TWS obtained from the extension of TWSA recorded five of
37 the seven extreme meteorological drought events in Yunnan Province from 1961 to
38 2001, therefore, the reliability of the expanded TWSA is better than GLDAS TWSA.
39 Generally, the findings of this study showed that the CP model using an innovative
40 input selection strategy is a useful and powerful tool for monthly TWSA prediction.

41 **Keywords:** GRACE; Total water storage anomalies; Support vector machine;
42 Combined prediction model; Input selection strategy

43 **1. Introduction**

44 The Gravity Recovery and Climate Experiment (GRACE) satellite, designed and
45 developed by the National Aeronautics and Space Administration (NASA) and the
46 German Aerospace Center (DLR), was launched on March 17, 2002. The monthly
47 changes in the Earth's gravity field observed by the GRACE mission are related to
48 changes in the total water storage (Δ TWS), including surface water and groundwater,
49 soil moisture, and snow/ice (Wahr et al., 1998). Many studies have verified it using situ
50 data, model data, and remotely sensed data (Doell et al., 2014; Long et al., 2015). In
51 recent years, GRACE Δ TWS data have been used widely in many fields of science.
52 Now, GRACE is a strong tool for scientists in a few science fields (Wouters et al., 2014),
53 and it has been employed to estimate individual or multiple water storages for different
54 applications by several studies (Andrew et al., 2017; Eicker et al., 2016 and Reager et
55 al., 2015).

56 GRACE Δ TWS has proven to be an important tool for drought and flood
57 monitoring in the hydrological field (Long et al., 2014; Zhang et al., 2015). The
58 GRACE Δ TWS at different time intervals can be obtained from the GRACE total
59 water storage anomalies (TWSA). Although GRACE Δ TWS has been successfully
60 used in hydrological science, it still has limitations in its further application in drought
61 and flood monitoring. GRACE's monthly TWSA data cover the period from 2002 to
62 2016, and there are 13 months of data loss (Famiglietti et al., 2013). In the past ten
63 years, some studies have been conducted using GRACE Δ TWS for drought and flood
64 monitoring (Zhang et al., 2015). However, TWSA data before the GRACE launch is

65 also necessary to understand the long-term trends of Δ TWS. In addition, there may
66 not be reliable TWSA data between the period of the decaying orbit of current GRACE
67 satellites and the launch of the GRACE Follow-On Mission in 2018. Thus, there is an
68 urgent need to develop a model for expand GRACE data with high accuracy.

69 Pan integrated several hydrological variable data records of the water cycle and used
70 data assimilation technology to establish a water cycle data record set for 32 major river
71 basins around the world from 1984 to 2006 (Pan et al., 2012). In this data set, TWS
72 outside of the GRACE period is provided by the Variable Infiltration Capacity (VIC)
73 model, which does not include simulations of changes in groundwater reserves, so the
74 data may be missing the interaction between surface water and groundwater systems
75 information (Liang et al., 1994). de Linage used a simple statistical model to predict
76 TWSA data over Amazon by examining the anomalous changes in sea surface
77 temperature (SST) from the equatorial central Pacific (Niño 4) and tropical North
78 Atlantic (TNAI) (de Linage et al., 2013). Finally, the R^2 between TWSA and a
79 combination of Niño 4 and TNAI was 0.43 in the overall Amazon basin. Please note
80 that due to the location and number of observing stations, it is not always possible to
81 obtain complete water level data. Moreover, surface models (for example, VIC) usually
82 ignore the interrelationship between surface water and groundwater, which may make
83 the total water storage obtained by the model lose the accuracy. Therefore, data-driven
84 models (such as ANN, SVM) that can obtain satisfactory results using available data
85 can be used to extend TWSA. Long used monthly precipitation, monthly average
86 temperature, and soil moisture storage (SMS) to construct an ANN model, and made a

87 long-term forecast of TWSA of the Yunnan-Guizhou Plateau from 1979 to 2002 (Long
88 et al., 2014). However, it is well known that a large amount of data is required to build
89 a reliable and powerful ANN model, but the available monthly observation value of
90 TWSA is 159 months. Therefore, more research should be conducted to establish a
91 robust model for TWSA prediction.

92 Support vector machines (SVM) are particularly suitable for modeling small sample
93 data sequences (Cortes et al., 1995). It is based on the Vapnik-Chervonenkis (VC)
94 dimensional theory and the principle of structural risk minimization. In theory, it can
95 overcome local convergence and achieve a global optimal solution. The SVM has been
96 widely used in streamflow prediction (Huang et al., 2014; Meng et al., 2019 and Meng
97 et al., 2021). However, due to the short length of the available monthly TWSA, using a
98 single model for TWSA expansion will lead to uncertainty and instability. ANN has
99 been employed for the TWSA extension in the karst plateau of Southwest China (Long
100 et al., 2014). At the same time, SVM has a strong ability for small sample data
101 prediction. Therefore, in this paper, a combined prediction (CP) model (including SVM
102 and ANN) is constructed for monthly TWSA extension. Meanwhile, hydrology
103 variables (including streamflow, precipitation, evaporation, and SMS) were employed
104 as potential explanatory variables of monthly TWSA. However, there is a correlation
105 between these potential explanatory variables. In this paper, a flexible input selection
106 strategy that can eliminate the interdependence between potential explanatory variables
107 is established to find the best combination of explanatory variables for monthly TWSA
108 expansion.

109 Yunnan province, the study area, is one of the wettest regions in China, with a forest
110 coverage rate as high as 50% (Han et al., 2019). Most of GRACE's research on TWSA
111 focuses on the changes in groundwater reserves in the southwestern region and the karst
112 plateau, as well as the monitoring of droughts and floods, but rarely pays attention to
113 Yunnan Province (Long et al., 2014; Huang et al., 2019 and Long et al., 2015).
114 Especially at the end of 2009, Yunnan province experienced a once-in-a-hundred-year
115 drought, which caused huge losses to local production and life. Therefore, it is of great
116 significance to predict TWSA with higher prediction accuracy.

117 The objectives of this study are to (1) check the performance of the flexible input
118 selection strategy for monthly TWSA reconstruction extension, (2) built an optimal
119 combination of explanatory variables for monthly TWSA reconstruction and extension,
120 (3) explore the performance of the ANN, SVM, and the CP model for monthly TWSA
121 extension in Yunnan province using the optimal combination of explanatory variables.
122 The extension of long-term TWSA data is of great valuable for understanding the
123 impact of climate change on the hydrological cycle and provides inspiration for water
124 resource management in Yunnan province.

125 **2. Materials and Methods**

126 2.1 Study region

127 Yunnan Province (97.31°-106.11°E, 21.8°-29.15°N) covers an area of 394,100 km²
128 (Fig. 1). The climate of Yunnan belongs to the subtropical plateau monsoon type, with
129 clear distinctions between wet and dry seasons, and the temperature varies significantly
130 with the terrain. Yunnan Province has an average rainfall of 1258 mm for many years

131 and has abundant water resources. There are as many as 908 rivers with a runoff area
132 of more than 100 square kilometers (Jiang et al., 2018).

133 2.2 GRACE data, Climate data, Streamflow data, Soil moisture data

134 In this study, the research data GRACE was got from The University of Texas Centre
135 for Space Research (CSR) at <http://isdc.gfz-potsdam.de/grace-isdc/>. The monthly
136 GRACE data lost 13 months of values, and these missing values were filled in with the
137 month values on both sides of the missing data through mean interpolation.

138 There are 27 meteorological stations in the province. The monthly precipitation and
139 potential evaporation data (from January 1960 to December 2010) of these stations can
140 be downloaded from the China National Meteorological Information Center
141 (<http://data.cma.cn/>).

142 In addition, monthly streamflow data (from January 1960 to December 2010) was
143 collected from the hydrologic manual. Strictly control data quality during release.

144 In this study, rasterized soil moisture data from 1960 to 2010 was obtained from the
145 VIC model product. This production is obtained by the VIC model using the
146 meteorological factors of the China Meteorological Administration (CMA). The
147 monthly soil moisture data is obtained by averaging the rasterized soil moisture data in
148 each hydrological station.

149 2.3 Methods

150 2.3.1 Artificial neural network (ANN)

151 ANN is an intelligent algorithm designed by imitating the working mechanism of the
152 human brain. It consists of three parts: input layer, hidden layers, and output layer. ANN

153 also needs weights and activation functions to simulate biological neural networks. The
154 activation functions commonly used in the hydrology field are tangent, logistic, and
155 linear. Detailed theoretical information about ANN can be found in (Zhang et al., 2014
156 and Fang et al., 2018). In this paper, the ANN is developed with three layers. The
157 sigmoid function was employed as the transfer function, and the optimal number of
158 neurons in the hidden layer is 5 after several trying.

159 2.3.2 Support vector machine (SVM)

160 Cortes and Vapnik (1995) proposed the support vector machine (SVM) which is an
161 efficient machine learning tool for time series forecasting. SVM uses a kernel function
162 to map the input factors of a complex nonlinear problem to a high-dimensional space
163 to simplify the complex problem, thereby transforming the complex nonlinear problem
164 into a linear problem. SVM is built based on statistical learning theory, which can help
165 SVM to obtain the global optimal solution. Some many papers and books have
166 described the theory of SVM in detail (Yoon et al., 2016; Carrier et al., 2013; Ch et al.,
167 2013 and He et al., 2014), the description of SVM is omitted. The kernel function is the
168 key for SVM to solve complex prediction problems, so, it's important to choose a
169 suitable kernel function. The kernel function includes linear, sigmoid, Radial Basis
170 Function (RBF), and so on. In this paper, RBF is employed as the kernel function:

$$171 \quad K(x, x_j) = \exp(-\|x - x_j\|^2 / 2\sigma^2) \quad (1)$$

172 where σ represents the Gaussian noise level of standard deviation.

173 2.3.3 Combined Prediction model

174 Meanwhile, the combined prediction (CP) model was employed to predict monthly

175 TWSA. The combined prediction can be expressed as follows:

$$176 \quad Y = w_1 * X_1 + w_2 * X_2 \quad (2)$$

177 where Y is the prediction value of TWSA using combined prediction, X_1 is the
178 prediction values of SVM, X_2 is the prediction value of ANN, w_1 is the weight of the
179 prediction value of SVM, w_2 is the weight of the prediction value of ANN. In this paper,
180 the values of w_1 and w_2 are obtained by the Genetic algorithm (GA). The detail of the
181 combined prediction model is shown in Fig. 2.

182 2.3.4 Innovative input variable selection strategy

183 To select the optimal input variable for monthly SWA prediction, an innovative input
184 selection strategy is proposed. The detail of this strategy is demonstrated as follows:

- 185 1. The 13 lags of streamflow $\{S_t, S_{t-1}, \dots, S_{t-12}\}$, precipitation $\{P_t, P_{t-1}, \dots, P_{t-12}\}$,
186 evaporation $\{E_t, E_{t-1}, \dots, E_{t-12}\}$ and SMS $\{I_t, I_{t-1}, \dots, I_{t-12}\}$ will be used as candidate
187 input variables.
- 188 2. The correlation coefficient between $\{P_t, P_{t-1}, \dots, P_{t-12}\}$, $\{E_t, E_{t-1}, \dots, E_{t-12}\}$ and
189 output variables is calculated in MATLAB. Suppose $\{P_t, P_{t-1}, P_{t-3}, P_{t-5}\}$ and $\{E_{t-1}, E_{t-2}, E_{t-6}\}$
190 are the optimal input combinations of rainfall and evaporation.
- 191 3. To get optimal input variable, a partial correlation algorithm is employed to
192 calculate the partial correlation algorithm between streamflow $\{S_t, S_{t-1}, \dots, S_{t-12}\}$,
193 SMS $\{I_t, I_{t-1}, \dots, I_{t-12}\}$ and output variables. This algorithm can eliminate the
194 influence of precipitation and evaporation on streamflow and SMS, the algorithm
195 is as follows:

196
$$r_{x_i y \cdot x_j} = \frac{r_{x_i y} - r_{x_i x_j} r_{y x_j}}{\sqrt{(1 - r_{x_i x_j}^2)(1 - r_{y x_j}^2)}} \quad (3)$$

197 where $r_{x_i y}$ is the correlation coefficient between x_i ($\{P_t, P_{t-1}, P_{t-3}, P_{t-5}\}, \{E_{t-1}, E_{t-2}, E_{t-}$
 198 $6\}$) and output variables y , $r_{x_i x_j}$ is the correlation coefficient between x_i ($\{P_t, P_{t-1}, P_{t-}$
 199 $3, P_{t-5}\}, \{E_{t-1}, E_{t-2}, E_{t-6}\}$) and x_j ($\{S_t, S_{t-1}, \dots, S_{t-12}\}, \{I_t, I_{t-1}, \dots, I_{t-12}\}$), $r_{y x_j}$ is the correlation
 200 coefficient between x_j ($\{S_t, S_{t-1}, \dots, S_{t-12}\}, \{I_t, I_{t-1}, \dots, I_{t-12}\}$) and output variables. And
 201 $r_{x_i y \cdot x_j}$ is the partial correlation coefficient between x_j ($\{S_t, S_{t-1}, \dots, S_{t-12}\}, \{I_t, I_{t-1}, \dots, I_{t-}$
 202 $12\}$) and output variables excluding the influence of x_i ($\{P_t, P_{t-1}, P_{t-3}, P_{t-5}\}$ and $\{E_{t-1}, E_{t-}$
 203 $2, E_{t-6}\}$).

204 2.3.5 Performance assessment principles

205 The general standard proposed by Moriasi et al. (2007) was introduced to evaluate
 206 the predictive performance of the model. The standard recommends using the Nash-
 207 Sutcliffe efficiency (NSE) coefficient, the percentage of deviation (PBIAS) and the
 208 ratio of the root mean square error (RMSE) to the standard deviation of the observations
 209 (RSR). The NSE is defined as:

210
$$NSE = 1 - \frac{\sum_{i=1}^n (z_i - z_i^*)^2}{\sum_{i=1}^n (z_i - \bar{z})^2} \quad (4)$$

211 where \bar{z} is the average of the observations; z_i and z_i^* represent the i -th observation
 212 and predicted value, respectively; n is the length of observation.

213 The PBIAS is as Eq. (5).

214
$$PBIAS = \frac{\sum_{i=1}^n (z_i - z_i^*) \times 100}{\sum_{i=1}^n z_i} \% \quad (5)$$

215 PBIAS can be used to calculate how far the predicted value differs from the observed
216 value.

217 The RSR is shown in Eq. (6), where the RMSE between the predicted value and the
218 observed value is standardized based on the standard deviation of the observed value.
219 The value range of this indicator is from zero to positive infinity, with zero being the
220 best.

$$221 \quad RSR = \frac{RMSE}{STDEV} = \frac{\sqrt{\sum_{i=1}^n (z_i - z_i^*)^2}}{\sqrt{\sum_{i=1}^n (z_i - \bar{z})^2}} \quad (6)$$

222 The algorithms used in the proposed framework all can be easily implemented with
223 the help of Matlab software or other sciences software.

224 **3. Results and discussion**

225 3.1 The performance of SVM and ANN using correlation coefficient algorithm

226 In this paper, runoff, precipitation, evaporation, and SMS data are set to fourteen
227 scenarios (Table 1) to find the optimal combination of input variables. The performance
228 of SVM and ANN will be explored in fourteen scenarios. Meanwhile, two different
229 input variable selection strategies are used to obtain the best input scenario for TWSA
230 reconstruction and extension.

231 The performance of SVM and ANN in 14 scenarios using correlation coefficient
232 algorithm (CCA) are shown in Table 2. Table 2 shows that in Scenario 1 to Scenario 4,
233 SVM and ANN have the best performance in Scenario 4 (NSE 85.16% of SVM, NSE
234 81.33% of ANN). It is proved that SMS is the main factor affecting TWSA in Yunnan
235 province (Han et. al 2019). At the same time, in Scenario 4, the performance of SVM

236 is better than that of ANN, which proves that the predictive ability of SVM is better
237 than ANN under a small number of samples. Among the 14 scenarios, the performance
238 of SVM in scenario 10 is best, and the same results can be found for the performance
239 of ANN (NSE 89.00% of SVM, NSE 87.77% of ANN). Interesting results indicate that
240 evaporation also affected the TSWA in Yunnan province.

241 3.2 The performance of SVM and ANN using the innovative input selection strategy

242 However, CCA does not consider the interaction between input variables when
243 calculating the correlation coefficient between input variables and output variables,
244 which may mislead the determination of the best combination of input variables. Thus,
245 an innovative input selection strategy is proposed to eliminate the interaction among
246 input variables. Table.3 and Fig. 3 show the performance of SVM and ANN using
247 innovative input selection strategy in fourteen scenarios.

248 The results in Table. 3 and Fig. 3 show that in scenario 4 to 14, the performance of
249 SVM and ANN is improved after using the innovative input selection strategy. Table. 3
250 and Fig. 3 show that among the fourteen scenarios, the best performance of SVM
251 appears in scenario 13 (NSE is 93.06%), and the best performance of ANN also appears
252 in scenario 13 (NSE is 92.98%). The NSE values of SVM and ANN increased by 5.33%
253 and 6.70%, respectively. The results prove that when the input variables are not
254 independent, the innovative input variable selection strategy can improve the predictive
255 ability of the model.

256 Scenario 13 includes precipitation, evaporation, and SMS. The water balance
257 formula in the basin system is $P-R-E=\pm\Delta S$, in which P is precipitation, R is streamflow,

258 E is evaporation and ΔS is water storage of the basin. At the same time, TWSA is the
259 interannual variation of water storage (ΔS). Therefore, P, R, and E are the main factors
260 affecting TWSA in Yunnan province.

261 3.3 The performance of the combined prediction

262 Table 3 and Figure 3 show that in scheme 13, the performance of SVM is better than
263 that of ANN. However, in scheme 13, the performance of ANN is the best among the
264 14 schemes. Therefore, in order to make full use of the advantages of support vector
265 machines and artificial neural networks, a combined forecasting method is proposed.
266 The performance of CP and other models is shown in Fig. 4. The results in Fig. 4 show
267 that the performance of CP in scenario 13 is better than that of SVM (the NSE value is
268 increase by 1.26%). Me, CP has the best performance among the five models under
269 scenario 13 (NSE is 94.25%, PBISA is -32.83, RSR is 0.24). At the same time, Long et
270 al. made predictions on the TWSA in the three regions of the Yunnan-Guizhou Plateau,
271 and the prediction accuracy was 91%, 83%, and 76%, respectively. In this study, the
272 NSE value of TWSA extension using CP model and innovative selection strategy is
273 94.25%, and the prediction accuracy of the model has been improved. The results prove
274 that the performance of CP in the reconstruction and expansion of TWSA is better than
275 that of a single model.

276 The extension values of monthly ΔTWS (1962~2001) obtained by CP using the
277 innovative selection strategy in Yunnan province are shown in Fig. 5. The results in Fig.
278 5 show that the monthly value of ΔTWS is the highest from June to August of the year,
279 while the monthly value of ΔTWS is lower from November to April of the year.

280 Meanwhile, the precipitation in Yunan Province is mainly concentrated from June to
281 August, accounting for 60% of the annual precipitation, while the precipitation from
282 November to April only accounts for 10-20% of the annual precipitation. The annual
283 change of the extended monthly Δ TWS values is highly consistent with the annual
284 change of precipitation in Yunnan Province, which proves the extension of TWSA is
285 reliable.

286 The annual Δ TWS value obtained by CP using the innovative selection strategy and
287 the annual Δ TWS value obtained by the Global Land Data Assimilation System
288 (GLDAS) are shown in Fig. 6. In the history of Yunnan province, there are seven
289 extreme meteorological drought events during 1961~2001, that are 1962/1963,
290 1968/1969, 1978/1979, 1980, 1983, 1987, and 1992 (Zheng et al., 2017). The results in
291 Fig. 6 show that the annual Δ TWS values obtained by CP catch five of seven extreme
292 meteorological drought events from 1961 to 2001. However, the annual Δ TWS value
293 obtained from GLDAS only captured three of seven extreme meteorological drought
294 events that occurred between 1961 and 2001. Moreover, the GLDAS Δ TWS value
295 only captures the beginning of two extreme meteorological drought events in
296 1968/1969 and 1978/1979 and failed to capture the water shortage in the middle and
297 late stages of these two drought events. At the same time, the annual Δ TWS values
298 obtained by the CP model also captured the two catastrophic floods that occurred in
299 Yunnan in 1991 and 1998, but the GLDAS Δ TWS value did not capture the two
300 catastrophic floods. Therefore, the accuracy of the TWSA extension obtained through
301 the CP model is higher than the TWSA of the GLDAS product obtained through the

302 physical model. Yunnan Province is located in a typical karst landform area, where
303 surface water and groundwater are closely connected. However, physical models may
304 ignore the interrelationship between surface water and groundwater, which may cause
305 distortion of the total water storage data they generate.

306 Figure 7(a) shows the correlation analysis between the monthly Δ TWS obtained
307 through the CP model and the monthly normalized vegetation index (NDVI) during the
308 verification period. As shown in Fig. 7(a), there is a significant negative correlation
309 between NDVI and Δ TWS. Fig. 7(b) shows the monthly NDVI anomaly value and
310 the monthly observation value of Δ TWS during the training period and the monthly
311 Δ TWS extension value during the verification period. As shown in Figure 7(b), during
312 the training period, the observed value of monthly Δ TWS is highly consistent with
313 the monthly NDVI anomaly value. At the same time, the monthly Δ TWS is also
314 highly consistent with the monthly NDVI anomaly value during the verification period.
315 The results in Figure 7 prove that the TWSA extension value obtained through the CP
316 model and the innovative input selection strategy has reliable accuracy. Therefore, in
317 Yunnan Province, the reliability of the TWSA expansion value obtained through the CP
318 model is higher than that of the GLDAS TWSA product. The results further proved that
319 the CP model using an innovative selection strategy has high accuracy for the extension
320 and reconstruction of TWSA in Yunnan Province.

321 **4. Conclusions**

322 The prediction accuracy and ability of the SVM, ANN, and CP using the innovative
323 selection strategy were explored by predicting monthly TWSA series in Yunnan

324 province in the present study. Meanwhile, fourteen scenarios of input variables were
325 explored to select an optimal input scenario for TWSA prediction. The performance of
326 the SVM was superior to the ANN due to its power prediction ability for a small sample
327 set. Of the fourteen scenarios, the performances of SVM and ANN using CCA in
328 scenario 10 (including evaporation and SMS) were optimal, and the performance of
329 SVM was better than that of ANN. The performances of SVM and ANN using the
330 innovative selection strategy were all better than that of SVM and ANN using CCA in
331 scenarios 5 to 14. In scenario 13 (including precipitation, evaporation, and SMS), SVM
332 using the innovative selection strategy performed best among fourteen scenarios (with
333 NSE 93.08%), and the same result was found in the ANN (with NSE 92.13%).
334 Therefore, input variables including precipitation, evaporation, and SMS are the
335 optimal input variables for TWSA prediction. Moreover, in scenario 13, the
336 performance of CP was superior to SVM and ANN using the innovative selection
337 strategy (with NSE 94.25%). Thus, CP with the innovative selection strategy has good
338 stability and high prediction accuracy for TWSA prediction. Therefore, this study
339 provides a superior choice for monthly TWSA prediction. TWSA is a significant tool
340 for the monitor drought and flood, providing a model with high prediction accuracy is
341 extremely meaningful for disaster prevention and mitigation.

342 **Acknowledgements**

343 This study was jointly funded by the National Key Research and Development
344 Program of China (grant number 2017YFC0405900), the National Natural Science
345 Foundation of China (grant number 51709221), the Planning Project of Science and

346 Technology of Water Resources of Shaanxi (grant numbers 2015slkj-27 and 2017slkj-
347 19), the China Scholarship Council (grant number 201908610170), the Open Research
348 Fund of State Key Laboratory of Simulation and Regulation of Water Cycle in River
349 Basin (China Institute of Water Resources and Hydropower Research, grant number
350 IWHR-SKL-KF201803) and the Doctorate Innovation Funding of Xi'an University of
351 Technology (grant number 310-252072007).

352

353 **Ethics declarations**

354 **Conflict of interest**

355 The authors have no conflicts of interest to declare.

356

357 **Ethical Approval**

358 Not applicable.

359

360 **Consent to Participate**

361 Not applicable.

362

363 **Consent to Publish**

364 Not applicable.

365

366 **Authors Contributions**

367 Conceptualization: S. H; E. M. Methodology: E. M; W. F. Formal analysis and

368 investigation: E. M; L. C. Writing - original draft preparation: E. M. Writing - review
369 and editing: E. M. Supervision: Q. H.

370

371 **Competing Interests**

372 None

373

374 **Available of data and materials**

375 Authors agree with data transparency and undertake to provide any required data and
376 material.

377

378 **References**

- 379 Andrew, R.; H. Guan; O. Batelaan. Estimation of grace water storage components by temporal
380 decomposition. *Journal of Hydrology*. **2017**, 552, 341-50.
- 381 Cortes, C.; V. Vapnik. Support-vector networks. *Machine learning*. **1995**, 20, 273-97.
- 382 Carrier, C.; A. Kalra; S. Ahmad. Using paleo reconstructions to improve streamflow forecast lead time
383 in the western u nited s tates. *JAWRA Journal of the American Water Resources Association*. **2013**,
384 49, 1351-66.
- 385 Ch, S.; N. Anand; B. K. Panigrahi; S. Mathur. Streamflow forecasting by svm with quantum behaved
386 particle swarm optimization. *Neurocomputing*. **2013**, 101, 18-23.
- 387 de Linage, C.; J. Famiglietti; J. Randerson. Forecasting terrestrial water storage changes in the amazon
388 basin using atlantic and pacific sea surface temperatures. *Hydrology & Earth System Sciences*
389 *Discussions*. **2013**, 10, 12453–83.
- 390 Doell, P.; H. Mueller Schmied; C. Schuh; F. T. Portmann; A. Eicker. Global - scale assessment of
391 groundwater depletion and related groundwater abstractions: Combining hydrological modeling with
392 information from well observations and grace satellites. *Water Resources Research*. **2014**, 50, 5698-
393 720.
- 394 Eicker, A.; E. Forootan; A. Springer; L. Longuevergne; J. Kusche. Does grace see the terrestrial water
395 cycle “intensifying”? *Journal of Geophysical Research: Atmospheres*. **2016**, 121, 733-45.

396 Famiglietti, J. S.; M. Rodell. Water in the balance. *Science*. **2013**, 340, 1300-01.

397 Fang, W.; S. Huang; Q. Huang; G. Huang; E. Meng; J. Luan. Reference evapotranspiration forecasting
398 based on local meteorological and global climate information screened by partial mutual
399 information. *Journal of Hydrology*. **2018**, 561, 764-79.

400 He, Z.; X. Wen; H. Liu; J. Du. A comparative study of artificial neural network, adaptive neuro fuzzy
401 inference system and support vector machine for forecasting river flow in the semiarid mountain
402 region. *Journal of Hydrology*. **2014**, 509, 379-86.

403 Huang, S.; J. Chang; Q. Huang; Y. Chen. Monthly streamflow prediction using modified emd-based
404 support vector machine. *Journal of Hydrology*. **2014**, 511, 764-75.

405 Han, Z.; S. Huang; Q. Huang; G. Leng; H. Wang; L. He; W. Fang; P. Li. Assessing grace-based
406 terrestrial water storage anomalies dynamics at multi-timescales and their correlations with
407 teleconnection factors in yunnan province, china. *Journal of Hydrology*. **2019**, 574, 836-50.

408 Huang, Z.; P. J.-F. Yeh; Y. Pan; J. J. Jiao; H. Gong; X. Li; A. Güntner; Y. Zhu; C. Zhang; L. Zheng.
409 Detection of large-scale groundwater storage variability over the karstic regions in southwest china.
410 *Journal of hydrology*. **2019**, 569, 409-22.

411 Jiang, Z.; R. Li; A. Li; C. Ji. Runoff forecast uncertainty considered load adjustment model of cascade
412 hydropower stations and its application. *Energy*. **2018**, 158, 693-708.

413 Liang, X.; D. P. Lettenmaier; E. F. Wood; S. J. Burges. A simple hydrologically based model of land
414 surface water and energy fluxes for general circulation models. *Journal of Geophysical Research:*
415 *Atmospheres*. **1994**, 99, 14415-28.

416 Long, D.; Y. Shen; A. Sun; Y. Hong; L. Longuevergne; Y. Yang; B. Li; L. Chen. Drought and flood
417 monitoring for a large karst plateau in southwest china using extended grace data. *Remote Sensing of*
418 *Environment*. **2014**, 155, 145-60.

419 Long, D.; Y. Yang; Y. Wada; Y. Hong; W. Liang; Y. Chen; B. Yong; A. Hou; J. Wei; L. Chen. Deriving
420 scaling factors using a global hydrological model to restore grace total water storage changes for
421 china's yangtze river basin. *Remote Sensing of Environment*. **2015**, 168, 177-93.

422 Long, D.; L. Longuevergne; B. R. Scanlon. Global analysis of approaches for deriving total water
423 storage changes from grace satellites. *Water Resources Research*. **2015**, 51, 2574-94.

424 Moriasi, D. N.; J. G. Arnold; M. W. Van Liew; R. L. Bingner; R. D. Harmel; T. L. Veith. Model
425 evaluation guidelines for systematic quantification of accuracy in watershed simulations.
426 *Transactions of the ASABE*. **2007**, 50, 885-900.

427 Meng, E.; S. Huang; Q. Huang; W. Fang; L. Wu; L. Wang. A robust method for non-stationary
428 streamflow prediction based on improved emd-svm model. *Journal of hydrology*. **2019**, 568, 462-78.

429 Meng, E; Huang, S; Huang, Q; Fang, W; Wang, H; Leng, G; Wang, L; Liang, H. A Hybrid VMD-SVM

430 Model for Practical Streamflow Prediction Using an Innovative Input Selection Framework. *Water*
431 *Resources Management*, **2021**, 35(4): 1321-1337.

432 Pan, M.; A. K. Sahoo; T. J. Troy; R. K. Vinukollu; J. Sheffield; E. F. Wood. Multisource estimation of
433 long-term terrestrial water budget for major global river basins. *Journal of Climate*. **2012**, 25, 3191-
434 206.

435 Reager, J. T.; A. C. Thomas; E. A. Sproles; M. Rodell; H. K. Beaudoin; B. Li; J. S. Famiglietti.
436 Assimilation of grace terrestrial water storage observations into a land surface model for the
437 assessment of regional flood potential. *Remote Sensing*. **2015**, 7, 14663-79.

438 Wahr, J.; M. Molenaar; F. Bryan. Time variability of the earth's gravity field: Hydrological and oceanic
439 effects and their possible detection using grace. *Journal of Geophysical Research: Solid Earth*. **1998**,
440 103, 30205-29.

441 Wouters, B.; J. A. Bonin; D. P. Chambers; R. E. Riva; I. Sasgen; J. Wahr. Grace, time-varying gravity,
442 earth system dynamics and climate change. *Rep Prog Phys*. **2014**, 77, 116801. 10.1088/0034-
443 4885/77/11/116801. <https://www.ncbi.nlm.nih.gov/pubmed/25360582>.

444 Yoon, H.; Y. Hyun; K. Ha; K.-K. Lee; G.-B. Kim. A method to improve the stability and accuracy of
445 ann-and svm-based time series models for long-term groundwater level predictions. *Computers &*
446 *Geosciences*. **2016**, 90, 144-55.

447 Zhang, X.-J.; Q. Tang; M. Pan; Y. Tang. A long-term land surface hydrologic fluxes and states dataset
448 for china. *Journal of Hydrometeorology*. **2014**, 15, 2067-84.

449 Zhang, Z.; B. Chao; J. Chen; C. R. Wilson. Terrestrial water storage anomalies of yangtze river basin
450 droughts observed by grace and connections with enso. *Global and Planetary Change*. **2015**, 126,
451 35-45.

452 Zheng, J; Wei, H; Yan, C; Zhou, J. Study on Meteorological Extreme-Drought Index for Yunnan
453 Province. *Plateau Meteorology*, 2017, 36(4): 1039-1051.

Figures

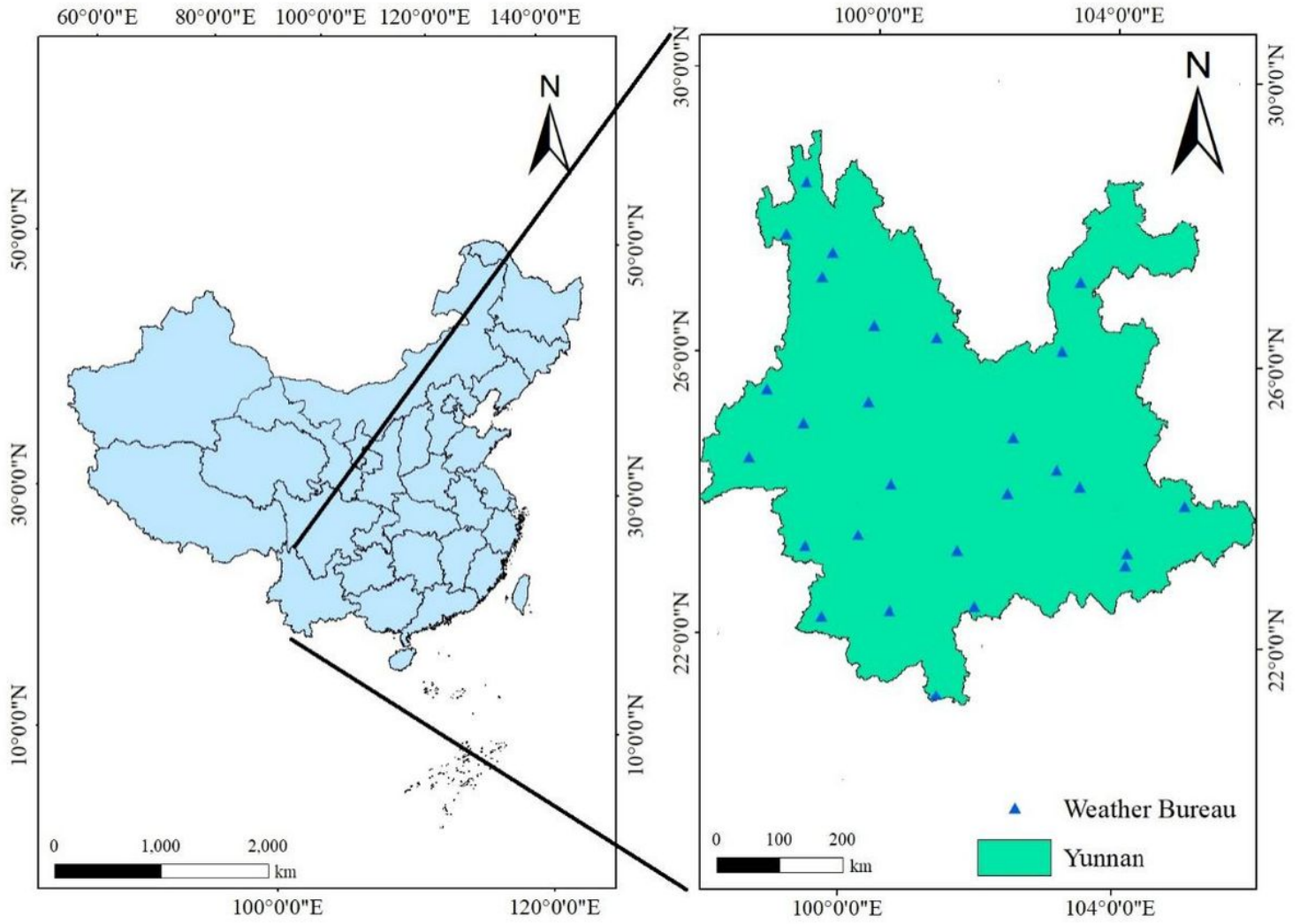


Figure 1

Location of the Yunnan province.

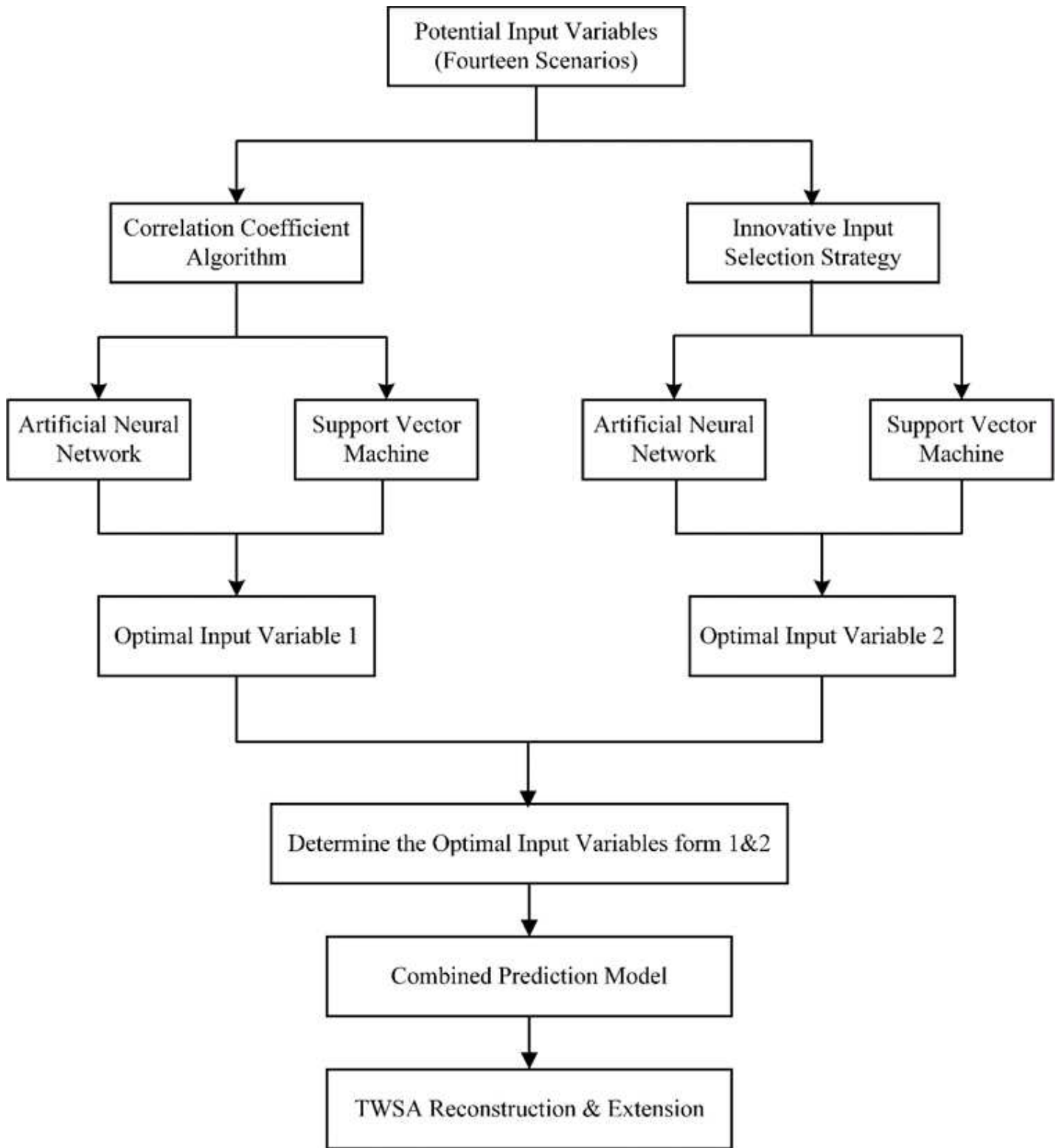


Figure 2

Flow chart of the Combined Prediction Model.

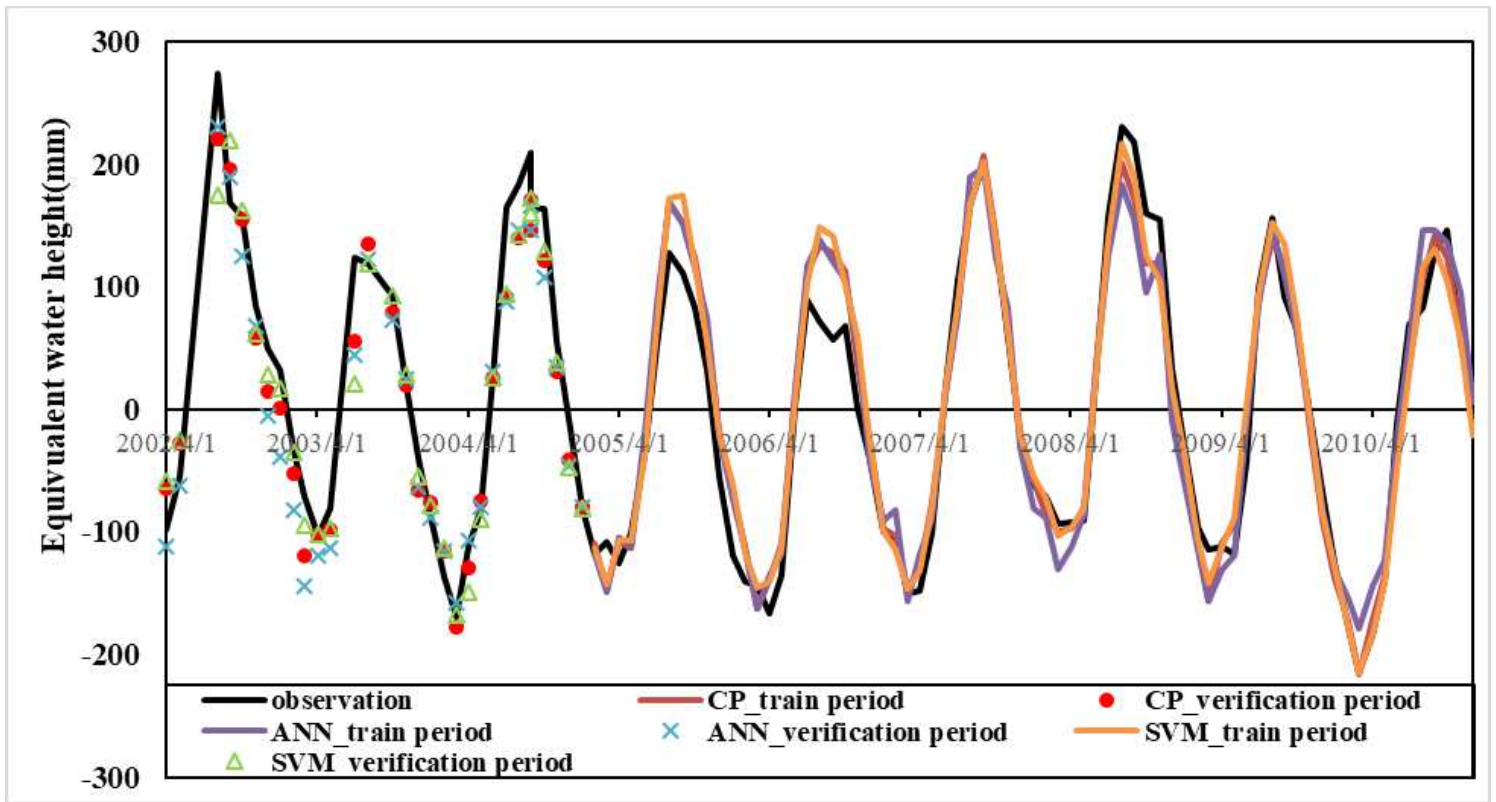


Figure 3

The performance of combined prediction (CP), ANN and SVM of TWSA using the innovative input selection strategy in test period and verification period.

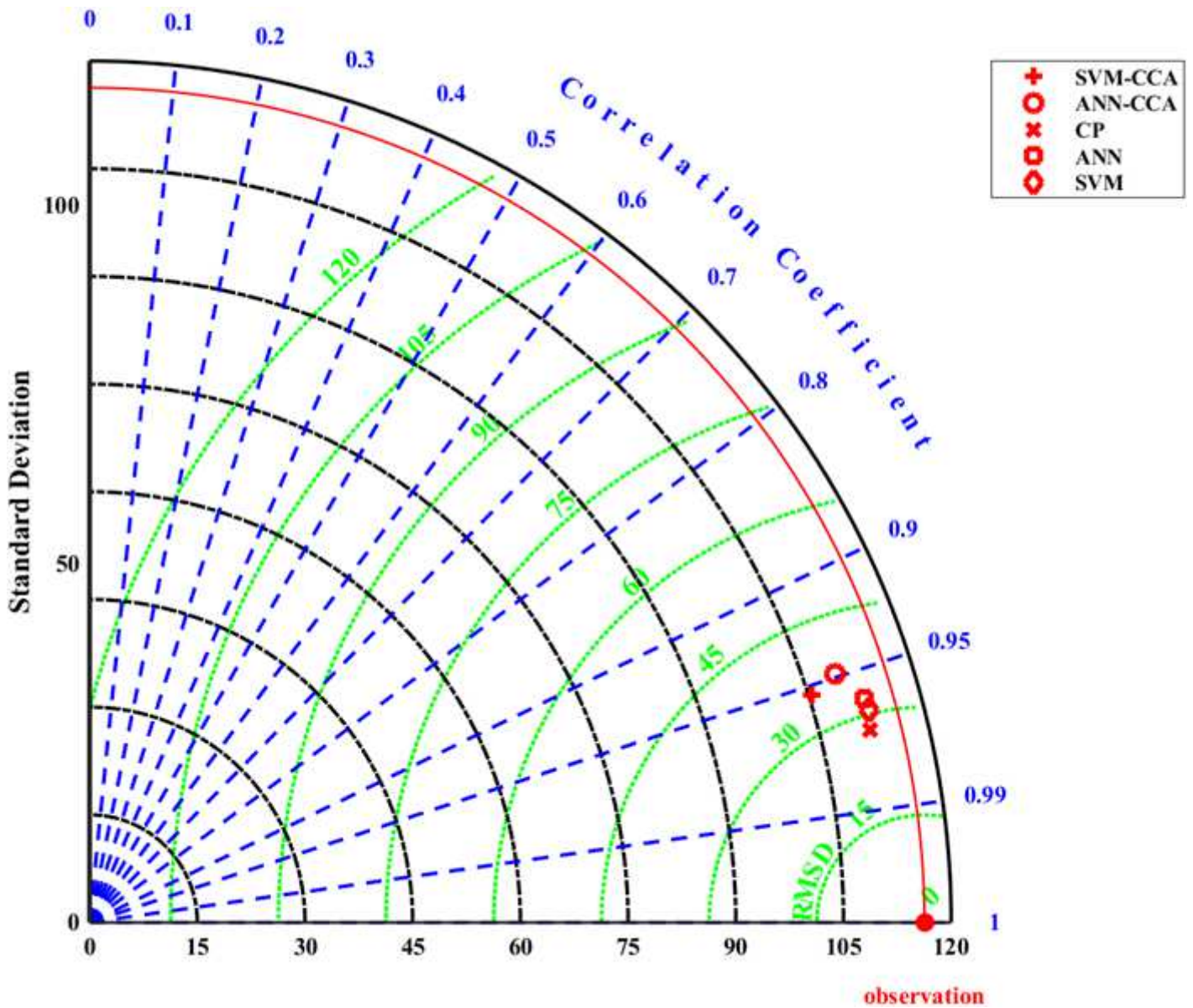


Figure 4

Taylor diagram of prediction by SVM and ANN using correlation coefficient algorithm (CCA), and combined prediction (CP), SVM, ANN using the innovative input selection strategy in verification period in Yunnan province where blue contours represent Pearson correlation coefficient; green contours represent centered RMS error in the simulated field; and black contours represent standard deviation of the simulated pattern.

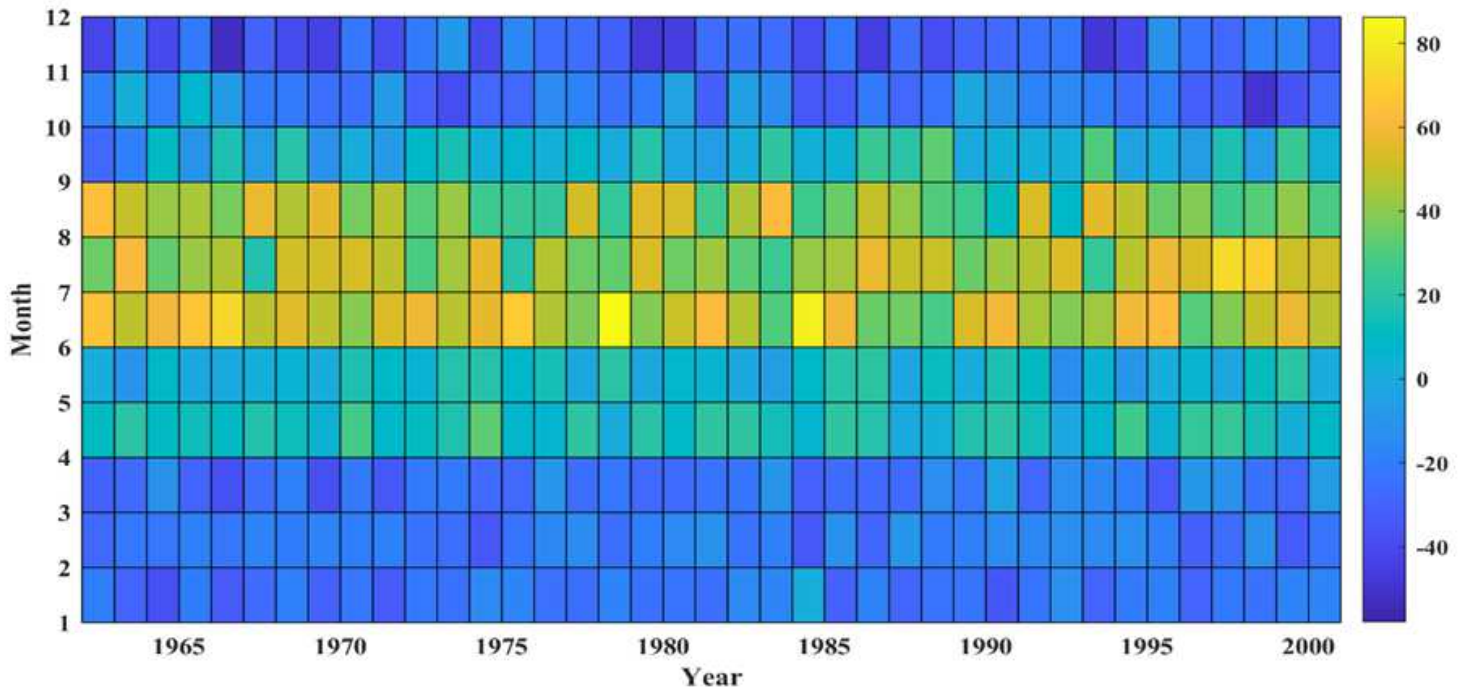


Figure 5

The monthly Δ TWS values obtained by CP using the innovative input selection strategy in Yunnan province.

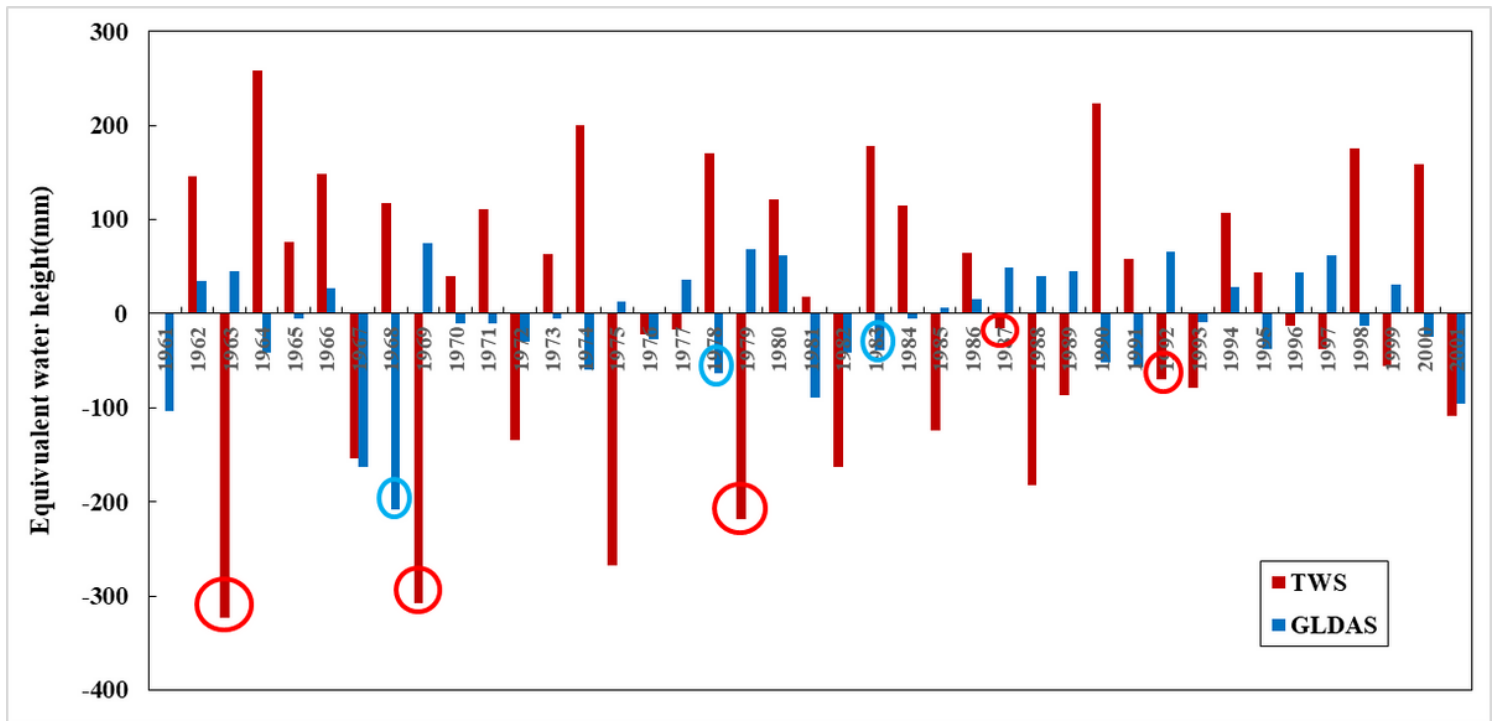


Figure 6

The annual Δ TWS values obtained by CP model using the innovative input selection strategy and GLDAS in Yunnan province

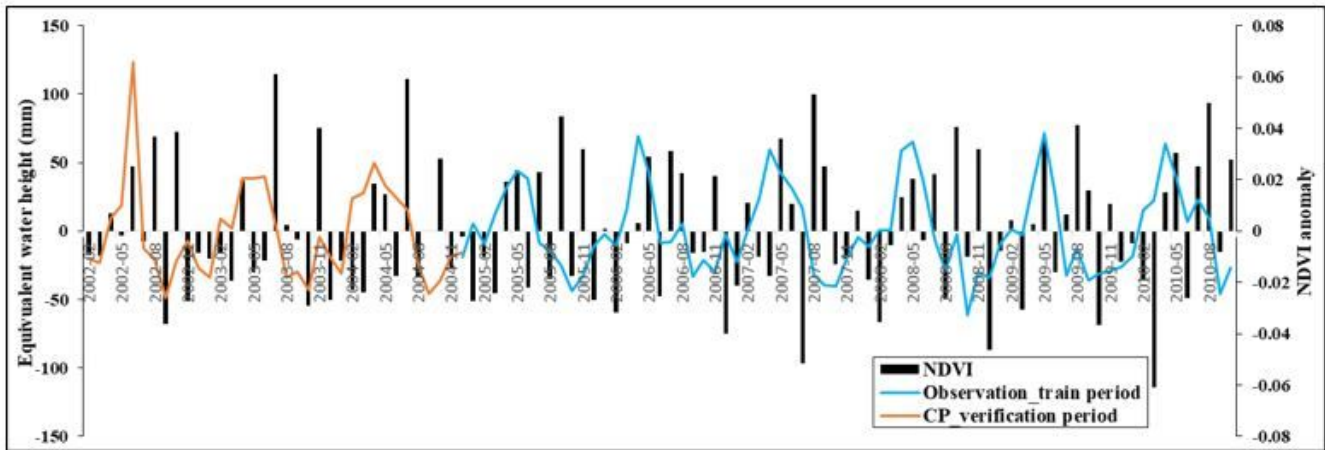
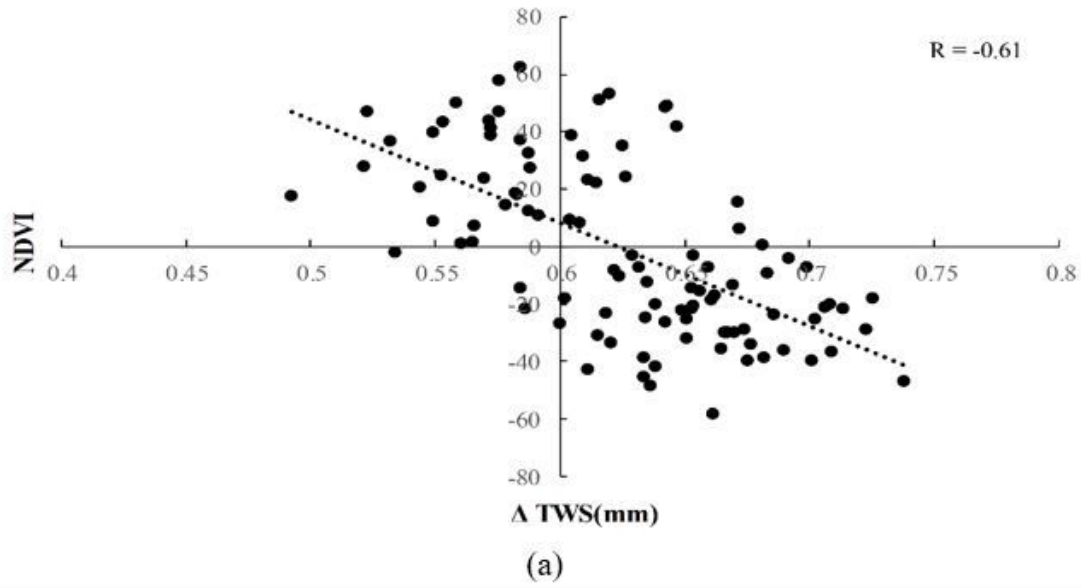


Figure 7

(a) The correlation analysis between monthly NDVI and monthly Δ TWS by CP model using the innovative input selection strategy in verification period; (b) The monthly NDVI anomaly and monthly Δ TWS.